New Families of Handed Shearing Auxetics via Parameterization

Andrew W. Kwa, Lillian Chin

***Abstract*— Handed shearing auxetics (HSAs) are a promising metamaterial for soft robotics, as their structure couples twisting with extension, enabling them to serve as an effective motor-driven transmission element. However, geometric exploration of HSAs has remained limited in scope, with no major design explorations performed on the HSA's unit cells. In this paper, we create a parameterization of the HSA's unit cells, simplifying the lattice structure to 13 key variables. This parameterization enables us to generate HSAs that outperform the original HSA in performance metrics like Poisson's ratio (8×), extension (3×) and actuation force (4×). We further demonstrate the versatility of this parameterization by creating a boundary curvature-inspired HSA gripper. Unlike previous HSA gripper designs that required 4 HSAs to function, our gripper has only requires a single HSA to achieve 8× the grasping force, taking advantage of the design flexibility offered by our tool. Overall, our parameterization significantly expands the potential mechanical design space of HSAs-powered soft robots.**

I. Introduction

Mechanical metamaterials are becoming an increasingly popular tool to design robots and improve their functionality [1]. Unlike traditional materials, which derive their mechanical properties from its internal chemical composition, mechanical metamaterials use *geometric structure* to achieve new mechanical properties. This geometric structure typically consists of a unit cell tessellated in a lattice formation. By changing the parameters of the unit cell or the tessellation, we can change the metamaterial's overall mechanical properties. This ability to program arbitrary mechanical properties has made metamaterials especially important in soft robotics, where tunable compliance and large-scale deformation are critical to robot performance [2].

Handed shearing auxetics (HSAs) have emerged as a particularly promising metamaterial for soft robotics [3]. HSAs are a subclass of auxetics — materials with a negative Poisson's ratio (ν) that become thicker when pulled. Auxetics do not occur naturally and can only be created as a mechanical metamaterial, where a single angle θ determines how much the auxetic expands (the "auxetic trajectory"). While auxetics are traditionally used in robotics as a passive constraint layer for fluidically-driven actuators [4]–[7], HSAs enable auxetics to serve as an *active* transmission element. Through the addition of chirality and shearing onto a cylinder, HSAs turn auxetics into a material that couples twisting with extension. When this twisting is provided by a motor's rotation, the HSA creates soft robotic actuators that are 2× faster at actuating and 20× more power efficient

All authors are with the Department of Electrical and Computer Engineering, University of Texas at Austin, TX, USA. Correspondence: akwa.2027@utexas.edu

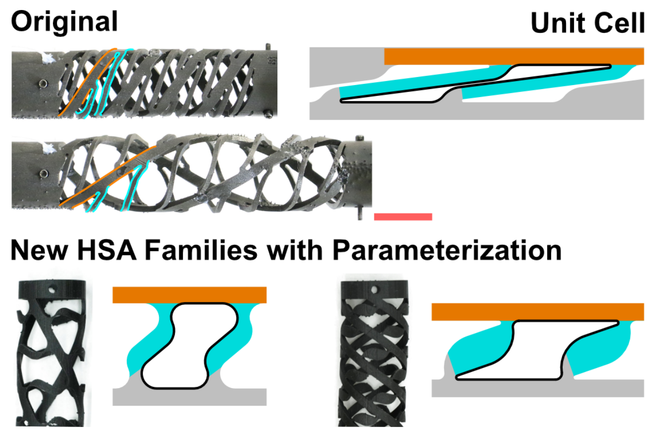

Fig. 1. (Top) Overview figure of the original handed shearing auxetic (HSA) pattern. Representative struts are highlighted in cyan and orange. The equivalent of these struts is highlighted in the same colors in the unit cell inset cartoon. The unit cell that will be used in this paper is the *negative space* between the cyan and orange struts, outlined in black. (Bottom) Representative handed shearing auxetics generated by our parameterized model. Varying the dimensions of the unit cell provides us significantly more control over the design of the resulting HSA. Scale bar (in red) is 2 cm and applies to all photos. Unit cells enlarged to show detail.

than traditional pneumatic soft robotic actuators [8]. HSAs dramatically increase the design space of soft robotic design, leading to their use in locomotion [9], [10], manipulation [11], [12], and brain-machine interfaces [13].

Surprisingly, HSAs have demonstrated this promise without engaging in the core benefit of metamaterials: tunability of mechanical properties through geometry. In all of the above citations of HSA usage, the core HSA unit cell geometry has not changed from its original 2018 introduction in [3]. This has led to a relatively large form factor in HSA designs, despite claims that the HSAs can be miniaturized down to the size of human vasculature [10], [14]. The lack of change to the unit cell has also presented challenges when different materials are used to fabricate the HSA [15]. The original HSA unit cell was designed for PTFE (polytetrafluoroethylene), which has an extremely large elongation at break (300-500%). Using the same unit cell design for more rigid materials leads to reduced robustness and premature fracture of the HSA, limiting its potential use. Although there have been some efforts to modify the HSA pattern [15], [16], efforts have been largely limited to changing:

- N, the number of copies of the unit cell pattern
- The initial θ, the position the HSA initially starts on the auxetic trajectory
- Cylinder parameters like thickness T and diameter $2r$

None of these efforts change the unit cell of the HSA itself, limiting the extent of robot design space exploration.

In this paper, we address this need by creating a parameterized model of HSA that simplifies the design of all potential HSAs down to 13 defining variables. Our parameterization translates the complex symmetry group-based conceptualization of HSAs in [3] into an easy-to-modify framework. We use this parameterization to create an algorithmic design tool that can quickly create HSA designs for different actuator needs. We use this tool to create new families of HSAs, each of which outperforms the original HSA design in key metrics like extension (3×), actuation force (4×), and Poisson's ratio (8×). As a final demonstration, we take advantage of the expanded HSA design space to create a novel HSA gripper that uses boundary curvatures to grasp objects in a kirigami-inspired way [17], achieving a grasping force 8× greater than previous HSA gripper designs. Overall, our work lays the foundation for the larger-scale design of HSA creation with significantly more speed, robustness, and control than previous methods. We make the following contributions:

1) We create a 13 variable HSA parameterization framework, enabling rapid prototyping of new HSA designs.
2) We demonstrate the versatility of the framework by creating new HSAs that surpass the original design in 5 key mechanical properties.
3) We demonstrate the increased design space provided by the framework by presenting a new single-HSA gripper with a grip force of 24 N, outperforming previous HSA grippers by 8×.

II. Methods

In this section, we describe how we algorithmically generate and fabricate the HSAs. We convert the original group theory-based model of HSAs described in [3] into a simple parameterized model to prioritize rapid prototyping.

A. Parametrizing the HSA: Unit Cell and Cylinder

The original description of HSAs focused on how symmetry groups could be leveraged to intentionally create chiral versions of existing shearing auxetics. In pursuit of these symmetry goals, an HSA's unit cell was defined as an N-shaped pattern that would be tiled across the surface of a cylinder (Fig. 2 of [3]). Upon full extension of the HSA cylinder, this N-shaped structure forms a "ladder"-like structure on the surface of the cylinder. The long struts of the N rotate to vertical "rails" that align with the cylinder axis, while the diagonal strut of the N rotates to become a "rung" of this metaphorical ladder. The rail and rung strut types are highlighted in orange and cyan, respectively, in Fig. 1.

We define a new unit cell according to the *negative space* formed by these two struts types. This unit cell definition is motivated by the flexure joints between the two strut types. Living hinges are a class of flexure joints that are created by narrowing down a material to a thin strip. The narrowing is defined by two opposing circles R_1 and R_2 that provide the radius of curvature for bending [18]–[20]. We define our new HSA unit cell based on these negative space circles.

We follow the variables defined in Fig. 2 to explain our unit cell construction. First, we set an initial bending radius

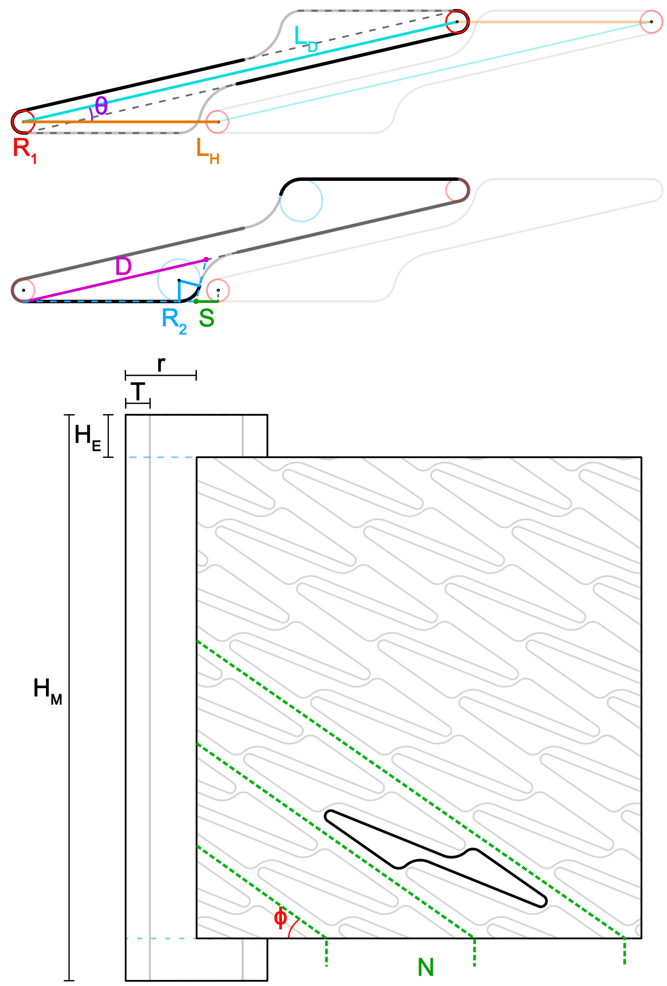

Fig. 2. Construction of the HSA unit cell and cylinder. (Top) The rough area of each unit cell is defined by translating circle R_1 by L_H horizontally and by L_D diagonally at a angle of θ. (Middle) The living hinge of each unit cell is defined by a spline defined by D, S and R_2. (Bottom) Each unit cell is tiled N times at an angle of ϕ. This pattern is wrapped around a cylinder of height H_M, radius r and thickness T. Sections of length H_E are reserved on either side of the cylinder to mount the HSA to fixtures.

of curvature R_1. We tile this circle in a parallelogram pattern, translating horizontally by L_H and diagonally by distance L_D at an angle of θ (Fig. 2-Top). L_H corresponds to a segment of the rail struts highlighted in orange in Fig. 1, while L_D corresponds to a segment of the rung struts highlighted in cyan in Fig. 1. θ is the main variable that changes as the HSA moves through its auxetic trajectory. We set θ according to the state within the auxetic trajectory in which we want our HSA to start. This first step of construction defines both the overall shape of the unit cell as well as the location of the next cell in the pattern. The side lengths of the unit cell will be defined as lines parallel to L_H and L_D that are tangent to the two R_1-sized circles in the unit cell.

Next, we will define the spline of the unit cell's flexure joint (Fig. 2-Middle). We define two points, D and S. D is a point that is a distance D along the L_D side of the unit cell from our initial R_1 circle. S is a point S away from the horizontally translated R_1 circle, along the L_H side of the unit cell. We use points D and S to construct the second circle of our living hinge joint. Specifically, we construct a circle with radius R_2 that is tangent both to L_H and the line segment $\overline{DS}$. We take the arc between those two tangent points and connect it to the L_H side of the unit cell. To complete the unit cell, we construct another arc that is tangent both to the L_D side and the line segment $\overline{DS}$. Since this arc is fully defined by the variables R_2, D and S, we do not specify another variable for its radius.

To create a full HSA cylinder, we take the unit cell pattern and tile it in a rectangular pattern (Fig. 2-Bottom). Let us define an HSA cylinder as having height H_M and radius r and thickness T. We reserve the H_E ends of the cylinder for interfacing, leaving us with a pattern space that is $H_M - 2H_E$ in height and r in radius. To pattern the unit cell onto the cylinder, we "unroll" the pattern space to be a rectangle of height $H_M - 2H_E$ and width $2\pi r$. To ensure that the pattern is continuous when the rectangle is "re-rolled", we specify N, the number of integer copies of the unit cell we tile. We also tilt the pattern by ϕ from the radial axis of symmetry of the cylinder, ensuring that we will achieve the desired "handed" property of the HSA.

These 13 variables fully define the HSA pattern and behavior. For example, the core spline of the flexure joint can be tuned by modifying R_1, R_2, D, S while leaving the main size of the unit cell unchanged. In this paper, we manually choose each parameter, although this framework can easily be used in a computational design pipeline. As a human designer, we approach modifying the variables as a means to modify the rail and rung struts. For example, by basic trigonometry, the rail strut thickness is equal to $\frac{2\pi r}{N}\sin\phi - L_D \sin\theta - 2R_1$, while the rung strut thickness is equal to $L_H \sin\theta - 2R_1$. Although both R_1 and θ appear in both equations, these variables have a much greater effect on the rung thickness than the rail thickness, due to more variables being present in the rail strut equation. Since the parameters are tightly coupled, in practice, we designed each HSA by modifying specific variables to affect specific features, such as R_1 and θ for rung strut thickness. We would then compensate their unintended effects on other features by tweaking the other variables. A more detailed discussion of variable selection is described in Sec. III.

B. HSA Generation and Fabrication

To fabricate the HSAs, we programmed the above parameterization in Rhino 8 and Grasshopper (Robert McNeel & Associates). These programs allow for easy access to our key parameters to generate STLs for 3D printing. To generate the STL, we follow the process outlined in Fig. 3. We first create the unit cell according to the construction in Fig. 2-Top and -Middle. We simultaneously create the rectangular pattern surface described in Fig. 2-Bottom of height $H_M - 2H_E$ and width $2\pi r$. We then tile the unit cells into a 2D array according to variables L_H, N and ϕ. This 2D array is made large enough that the rectangular pattern surface can be contained entirely within the array. We then perform a Boolean subtraction of the 2D array from the rectangular pattern, thus creating the holes / negative space

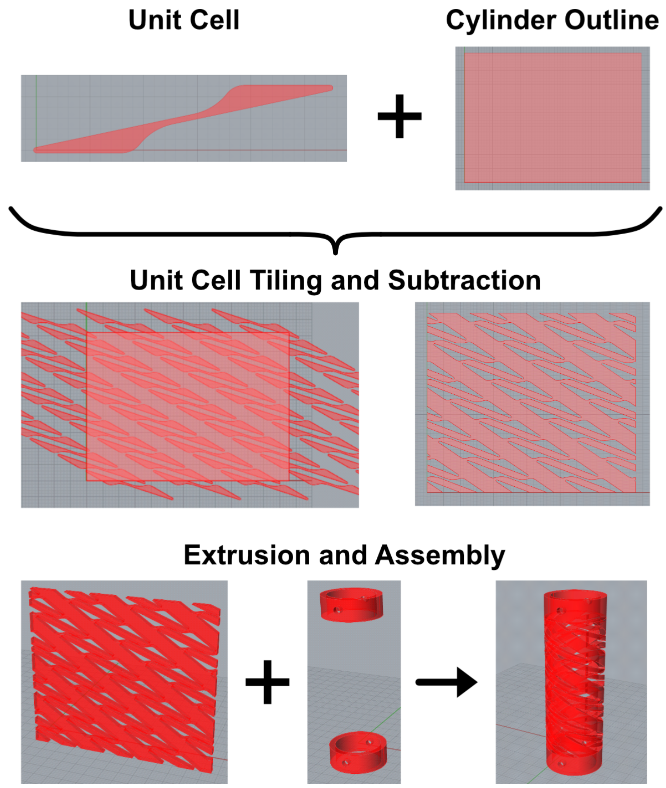

Fig. 3. Walkthrough of the HSA generation algorithm. After constructing the unit cell and the outline of the pattern area of the cylinder, we tile the unit cell across the pattern surface. We then perform a boolean subtraction of the unit cell tiling from the pattern outline, creating the cylinder surface once the pattern outline is extruded. We finally wrap the pattern outline into a cylinder and attach the end caps to form the full HSA.

of the HSA. This cut surface is then extruded by thickness T and wrapped into a cylindrical shape. Finally, we separately construct the end caps of the HSA to attach to the pattern surface. These end caps have height H_E, thickness T and radius r and may be customized for mounting purposes (ex. bolt clearance holes). All of these components are assembled and exported as a single cylinder STL.

We use the STLs to print HSA cylinders out of TPU 95A (Thermoplastic polyurethane, Bambu Carbon X1C) and FPU 50 (Flexible polyurethane, Carbon M2). TPU 95A was chosen as it is a highly flexible and durable elastomer that can easily recover from high deformation, while FPU 50 was chosen because it is a semirigid material which can withstand repeated stresses. The many thin components of the HSA and the flexibility of TPU and FPU meant that support struts were a major design consideration. Difficulty in removing support material limited how thin we could make flexure joints and small struts, affecting what parameters we could ultimately use in our design. To improve support removal, HSAs were printed on their side. Overall, the algorithmic tool created a design pipeline that was easy to modify, allowing us to easily iterate for fabrication challenges and performance needs.

III. Creation and Characterization of New HSAs

In this section, we explore the metamaterial design space that is made accessible by our parameterization tool. To do

TABLE I

LIST OF GENERATED HANDED SHEARING AUXETICS

Material	HSA Design	Cell Variables							Cylinder Variables					
		L_H (mm)	L_D (mm)	θ (°)	R_1 (mm)	R_2 (mm)	S (mm)	D (mm)	N	ϕ (°)	H_M (mm)	H_E (mm)	T (mm)	r (mm)
FPU, TPU	Original [3]	20	51.2	7.5°	0.3	1.5	1.75	20.5	3	23.62°	132	7	1.59	13
FPU TPU	Extension	12	35 30	6° 5.4°	0.15	0.5 0.75	0.75 0.6	12	3	12.5° 15°	132	7	1.59	13
FPU TPU	Compression	16	20	40° 35°	3.5 1.75	5 3	2.25 2	10.5 12	3	60° 50°	132	7	1.59	13
FPU TPU	Force	15	35	10° 7.5°	0.3	0.75	1.5	15	3	30°	142	12	2.25 3	13
FPU TPU	Small ν	20 30	55 60	6° 4.5°	0.1	1	1 1.5	21 30	6 5	37.5°	132	7	1.59	13
FPU TPU	Large ν	15	22.5	20°	0.3	1	1	20	4	35°	132	7	1.59	13
TPU	Gripper	36.4	183.4	6°	0.4	5	7	45	2	35°	100	10	2	15

so, we translated the original HSA design from [3] into our new negative space unit cell framework and used that as a starting point for new manually created HSA variants. To ensure a fair comparison across HSAs, we keep the pattern surface constant across all HSAs. In this section, all HSAs have a pattern surface of height $H_M - 2H_E = 118$ mm and width $2\pi r = 81.7$ mm. All other parameters were changed by trial and error to achieve better performance. Table I describes the resulting HSA patterns.

Although the unit cell describes the negative space / holes of the HSAs, our intuition for selecting dimensions was based on the shape and size of the lattice struts and living hinges. For example, FPU and TPU have dramatically different material properties from one another and the original PTFE material for HSAs [3], [15], [21]. Since TPU is more flexible than FPU, TPU-based designs generally needed thicker struts (smaller L_D and larger ϕ for rail struts, smaller R_1 for rung struts) to avoid structural instability. Meanwhile, since FPU is more rigid than TPU, FPU-based designs needed thinner flexure joints (smaller S) to avoid snapping during extension. These material changes result in different parameter values across Tab. I, especially from the original PTFE-based HSA parameters. Through an empirical design approach, we created HSAs that improved upon the original HSA design in four different mechanical properties:

1) Extension length
2) Compression length
3) Force required to extend
4) Poisson's ratio

We characterized properties (1), (3) and (4) by conducting a tensile test to failure (Shimadzu AGS-X). Property (2) was characterized by conducting a compression test to 80 mm with the same testing machine. For all tests, the top end of the HSA was mounted to the standard tensile / compression testing platforms using a custom 3D printed fixture (PLA (polylactic acid), Bambu Carbon X1C). Meanwhile, the bottom end of the HSA was attached to a custom fixture that allowed free rotation of the HSA during testing. This fixture was made of a combination of bearings, laser cut acrylic and 3D printed PLA parts. We allowed rotation to ensure that the metamaterial pattern would be engaged during testing. Three trials for each condition were attempted, which we use to report the average and standard deviation.

A. High Extension HSAs

To achieve high extension, we recognize that the distance the HSA can extend is dependent on the ratio between the initial starting length of the HSA pattern ($H_M - 2H_E$) and the length of the HSA's rail struts ($\frac{H_M-2H_E}{\sin\phi}$). The longer the rail strut is relative to the initial HSA pattern length, the farther the HSA can extend. Since this ratio is equivalent to $\frac{1}{\sin\phi}$, we can achieve a longer extension by decreasing ϕ.

To accommodate the longer rail struts, we also need to shrink each unit cell, which we do by decreasing θ, L_D, L_H. We could also have achieved this by decreasing N, but found that this resulted in an unstable structure. This shrunken unit cell requires tweaking the flexure joint to still work at the smaller geometry, leading us to modify R_1, R_2, S, D as well.

We found that the FPU extension HSA achieved 3× the length of the FPU base HSA (536.2 ± 83.7 mm vs. 180.1 ± 22.1 mm), as seen in Fig. 4. Likewise, the TPU extension HSA performed on average better than the original (617.3 ± 160.2 mm vs. 355.1 ± 58.8 mm), with one test even reaching the tensile tester's limit of 750 mm. This performance improvement existed despite the TPU extension HSA displaying significantly greater variability than the TPU original HSA (σ_{ext} = 160.2 vs σ_{orig} = 58.8). We believe this variability is because of differences in print quality, especially since the very thin rung struts would easily break and were susceptible to poor layer adhesion.

B. High Compression HSAs

Similar to the high extension HSAs, the distance an HSA will compress is dependent on the ratio between the rail strut length to the initial starting length of the HSA pattern area. The shorter the rail strut is to the initial length, the more the HSA is able to compress. This means that we want to *increase* ϕ so that $\frac{1}{\sin\phi}$ can be as small as possible. We also note that the HSA's starting state must be in the most open part of its auxetic trajectory, meaning that θ must be larger than its usual low, near-closed state. To maximize the length

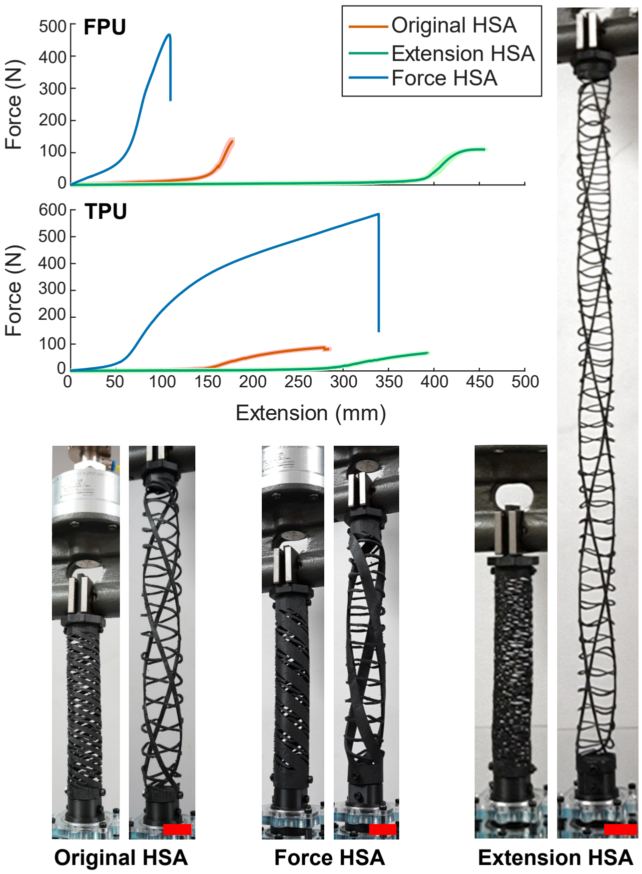

Fig. 4. Tensile tests comparing the original HSA with high force and extension versions. (Top) Summary of all tests for both FPU and TPU. Error bars are standard deviation from 3 trials. (Bottom) Sample tensile test demonstrations of FPU-based HSAs. Scale bars are 2 cm.

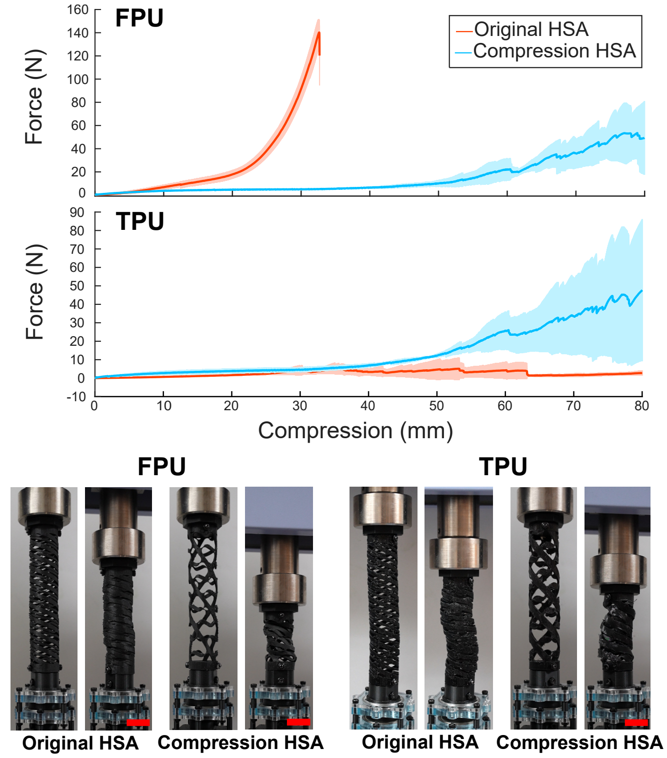

Fig. 5. Compression test comparing the original HSA with the compression version. (Top) Summary of compression tests for both FPU and TPU. Error bars are standard deviations from 3 trials. (Bottom) Compression test demonstration on FPU and TPU-based HSAs. Scale bars are 2 cm.

of travel during compression, we also make the rung struts of the HSA be as thin as possible. This creates a sparser strut architecture that will minimally impede HSA compression. We decrease the rung strut thickness by increasing R_1 and tune the flexure joints by modifying S, D, R_2.

From Fig. 5, we see that the FPU original HSA barely compresses before fracturing (32.6 $\pm$ 13.1 mm), as it is close to the closed state on the auxetic trajectory (low θ). The TPU original HSA begins buckling early in the compression (around 35 mm) due to TPU's high flexibility. This is noted by the initial dip in force in Fig. 5. The TPU original HSA continues to buckle outwards through the rest of the compression, explaining the smaller repeated dips in force. By contrast, the FPU and TPU compression-type HSAs compress relatively unimpeded, until approximately 50 and 60 mm of compression, respectively. At that point, the HSA is so compressed that the struts are compacted together and have little room to compress further. As a result, we see an increase in change in exerted force for the FPU HSA, while the TPU HSA begins to buckle due to its lower stiffness.

C. High Tensile Force HSAs

The force required to actuate an HSA is largely determined by the thickness of the rail struts. Since the rail struts rotate to vertical on full extension, they take on most of the loading of the full HSA cylinder. We made thicker rail struts by increasing ϕ and decreasing cell size, as well as increasing overall cylinder thickness T. The flexure joints also play a role in actuation force, by determining how easily the struts can rotate against one another. Increasing the joint thickness (larger S) will increase the amount of torque required to actuate, although care needs to be taken to not have the joint be so thick that it will snap rather than rotate.

Testing the high-force HSAs resulted in significant challenges. In our initial testing, the point of failure for the HSA would be at the mounting holes at the ends of the HSA. As a result, we increased H_E to give more material between the HSA ends and mounting holes, increasing H_M by a compensatory amount to preserve the same pattern height. After this modification, the PLA top test fixture sheared for both the FPU and TPU HSA designs. The tensile strength of PLA is 31 ± 3 MPa [22], meaning that our parameter modifications allowed us to surpass that with no ill effect to the HSA. Due to the fixture shearing, we only recorded one trial for this condition. Despite this limited analysis, we see from Fig. 4 that the high-force HSAs required significantly higher actuation force per distance than the original HSAs. This did not come at a noticeable loss in extension length.

D. Variable Poisson's Ratio HSAs

The HSA's Poisson's ratio (ν) is determined largely by the length and initial angle of the rung struts (L_D, θ).

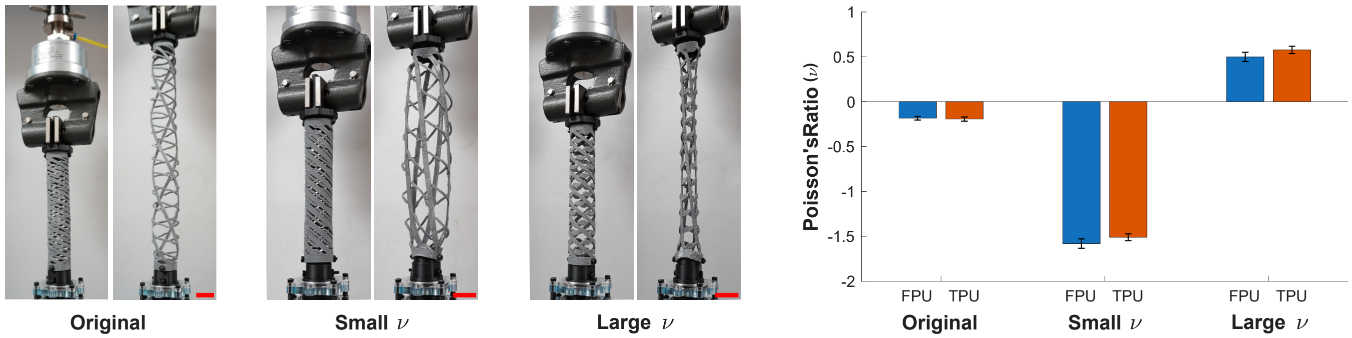

Fig. 6. Comparison of original HSA versus HSAs designed to have small / large Poisson's ratio (ν). (Left) Sample extension demonstrations of TPU-printed HSAs. (Right) Summary of all tests, both with FPU and TPU. Error bars are standard deviation from 3 trials. Scale bars are 2 cm.

Full extension of the HSA is determined by the rail struts becoming vertical. At that point of extension, the rung struts will rotate along the auxetic trajectory (increasing θ to θ_E, the value of θ when the HSA is fully extended), which will result in an effective lateral expansion of $L_D \sin\theta_E$. However, this expansion only occurs *if* the rung struts can sufficiently push the longer struts apart from one another. This occurs when the rung struts are sufficiently thick enough to resist bending / buckling (smaller R_1).

Thus, to design ν, we can think of the rung struts as providing a constraining curve to all of the rail struts. If $L_D \sin\theta_E$ is sufficiently large, there will be more room for the HSA to laterally expand. By contrast, if $L_D \sin\theta_E$ is too small, then the rail struts will be pulled closer together, resulting in a *positive* Poisson's ratio. Our HSA parameterization creates non-auxetic materials because our parameterization is targeted for *fabrication*, not directly translating the original paper's HSA unit cell formulation [3]. The original paper focuses on maintaining symmetry guarantees that lead to auxetic behavior, which our paper does not follow. We view this as a positive because it opens up the design space of HSAs to include non-auxetic metamaterial designs.

To create an HSA with a small ν (i.e. negative), we increase L_D and decrease R_1 to increase the rung strut length and thickness, respectively. R_2, S, D are tuned to have the flexure joint still perform well. We also increase ϕ to provide enough room to increase N. This enables us to have thinner rail struts for the rung struts to push apart, while maintaining sufficient stability in the entire HSA structure. Finally, we decrease θ so that we have more room to move in the auxetic trajectory (i.e. makes $\sin\theta_E$ as large as possible).

To create an HSA with a large ν (i.e. positive), we decrease L_D so that we quickly move past the auxetic trajectory and minimize the strength of the rung struts in driving the auxetic trajectory. We also increase θ so that we minimize time spent in the auxetic trajectory. In addition, we increase ϕ so that the rail struts reach their vertical state while the rung struts are still relatively early in their auxetic trajectory (i.e. θ is still small, so $\sin\theta_E$ remains small). Lastly, we increase N to create thinner rail struts that the rung struts can influence when they move past the auxetic trajectory.

With these modifications, the small-ν HSA increased the magnitude of the original HSA's ν by $8\times$ (Fig. 6-Right). In addition, the large-ν TPU HSA has a positive Poisson's ratio larger than TPU's natural Poisson's ratio (0.58 ± 0.04 vs. 0.48, according to [23]). In summary, these characterization experiments have outlined a set of design principles to modify existing HSAs for specific mechanical needs.

IV. Design and Demonstration of HSA Gripper

In this section, we take the parameterization lessons learned from Sec. III to create a unique HSA gripper that only requires a single HSA, unlike previous efforts that required 4 HSAs [8], [11]. We do so by taking a similar grasping approach to the boundary curvature gripper introduced in [17]; we place a single geometric object between two fixed ends and provide an actuation input. In [17], they applied a linear pull to kirigami. In this work, we apply a torque from two servos (GDW RS0708) rotating against each other on a single HSA. Both grippers work by creating a "pocket" through extreme negative Poisson's ratio that can envelop objects to lift them (Fig. 7).

A. Gripper Design

We design the gripper HSA using the small ν HSA from Sec. III-D as a starting point. Since the gripper HSA will be fixed on both ends, it does not need the same structural stability that the small ν HSA required. This allows us to have weaker rail struts and rung struts, as they are no longer needed to drive the auxetic expansion. We set the rung struts to be very long (large L_D), enabling extremely large lateral expansion of the HSA. We also increase R_1 to ensure that the rung struts are thick enough to handle object weight without breaking. The last major design choice is to set $N = 2$, to create a single pocket / grasping zone for objects to enter for grasping. We manufacture this HSA out of TPU for the material's highly flexible yet durable properties.

To turn the HSA into a gripper, we 3D print PLA mounts which directly connect the HSA ends to the servo horns. The servos are fixed to a U-shaped mount made of laser cut acrylic plates with 3D-printed PLA L-brackets. Finally, we attach the mount to a 3D printed attachment with the hole pattern for a Franka Emika Panda robot arm. We control the gripper using an Arduino Uno to interface with the Panda arm and set the servos to open and close the HSA.

Fig. 7. HSA gripper demonstration, picking up a lens cap (highlighted in green). From left to right, the HSA twists open, the robot lowers onto the object, the HSA is twisted closed, and the robot lift the object up. Scale bar is 2 cm.

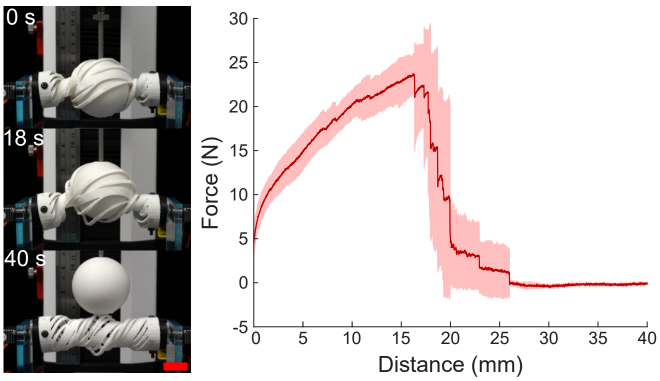

Fig. 8. Grip force characterization test. (Left) Snapshots of HSA gripper during testing. (Right) Summary of grip force tests for the HSA gripper. Error bars are standard deviation from 5 trials. Scale bar is 2 cm.

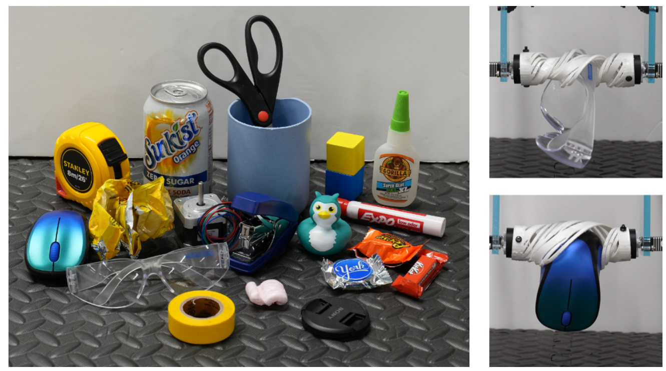

Fig. 9. (Left) Objects successfully grasped by the HSA gripper. The unusual geometry of the HSA gripper means that it can grasp objects in both (Top-Right) a pinch grasp and (Bottom-Right) a power grasp.

B. Gripper Characterization

To evaluate the HSA gripper, we conduct a grip force test and grasping tests of household objects. We characterize the grip force by measuring the force required to remove a 50 mm diameter 3D printed sphere from the gripper's grasp, following the same procedure outlined in [15]. We perform a tensile test using a universal testing machine (Mark-10 Series F+) where the gripper is fastened to the base and the sphere is attached to the load cell. The sphere is initially grasped by the gripper and pulled out of the gripper at a rate of 1 mm/sec. The test ends when the sphere is fully out of the gripper's grasp, leading to a sharp decrease in measured force. We normalize according to that final force, as it represents a true zero applied force. A total of 5 trials were conducted to report average and standard deviation.

From Fig. 8, we see that the gripper has an initial grasping force of 4.56 ± 1.52 and reaches a maximum average gripping force of 23.74 ± 2.29 N. Comparing to the 4-HSA based grippers presented in [15], we see that our maximum gripper force is nearly 8 $\times$ higher than what was previously reported (2.98 ± 0.39 N with a FPU gripper). This is because the boundary curvature style grasp creates more surface area between the HSA struts and the grasped object, providing a much stronger grasp.

Next, we evaluate the gripper's performance in grasping tests. We selected 18 everyday objects as manipulation targets (Fig. 9) and attempted to grasp them from rest on a table. We placed each object at a pre-set location and commanded the Franka arm to move vertically from that location using Cartesian commands. For each object, we manually applied variable grasping strengths based on how much we commanded the HSA servos to close. The objects we selected ranged in shape and size, weighing between 1 - 373 g and having lengths from 2.7 - 19.5 cm. Notably, our gripper HSA's initial radius was only 15 mm. We are only able to grasp large objects due to our very low ν making a large grasping pocket appear upon actuation.

We found that our gripper was able to grasp all objects tested, as the struts were able to surround and envelop the manipulation targets. In particular, the gripper excels at grasping objects with small ridges or crevices in which the HSA struts can lodge themselves (trash, tape measure). This was true even for relatively flat objects, such as the lens cap (Fig. 7), which usually require fingernails or forceful pinch grasps to lift. Indeed, the HSA gripper showed a surprisingly wide range of grasping diversity: performing delicate pinch grasps for small fragile objects (candy, packing peanut) and forceful power grasps for heavier objects (soda, tape measure, stepper motor).

We did note that slippage occurred for objects with smooth surfaces, such as the computer mouse, safety glasses and stapler. This is to be expected, as no friction features were printed onto the HSA structure under our parameterization. The safety glasses, in particular, posed a challenge for our gripper, as it was both smooth and larger than our grasping pocket. Ultimately, we had to rely on the glasses' geometric ridges (ex. nose bridge, hinges) to catch on the HSA's struts.

Future work could explore how HSA strut design could be optimized for these non-standard loading to the HSA. Overall, this grasping evaluation provides strong evidence that our parameterization tool enables us to explore new HSA morphologies that lead to better robotic performance.

V. Discussion

In this paper, we created a parameterization framework that dramatically increased the design space of HSAs. This space was previously unexplored due to the difficult symmetry group-based formulation of the original HSA paper. By breaking down HSA design into 13 variables, we are able to easily manipulate unit cells and lattice patterning to generate new families of HSAs. With this tool, we demonstrated five new HSA designs that exceeded the performance of the original HSA in key mechanical properties: extension, compression, force, small Poisson's ratio, and large Poisson's ratio. We also created a new soft gripper design which utilizes a single HSA to grasp a variety of household objects with a higher grasping force than previous HSA designs.

Through the process of generating HSAs, we are able to find trends associated with altering the parameters we set. We see that L_D alters the length of the rung struts, R_1 is inversely proportional to their thickness, and θ determines where they begin in their auxetic trajectory. The rail strut size can be increased with a larger ϕ and a small N. D, S, R_1, and R_2 tune the flexure joints for smooth rotation, while L_D determines the spacing / frequency of the rung struts. These observations allowed us to pursue a principled design approach to altering HSA behavior. A larger ratio of rail strut to HSA starting length ratio leads to longer HSA extension length, while a smaller ratio of rail strut to HSA starting length combined with sparser small strut density leads to a longer compression length. Larger / thicker rail struts leads to greater actuation force of the HSA. Finally, Poisson's ratio is determined by the rung struts. A longer length with a small θ results in a smaller ν and a larger θ leads to larger ν.

In the future, we will incorporate these manually-discovered design principles into a computational design loop. By tying the parameterization tool to a simulation loop, we will be able to discover the optimal HSA design for a given application. We will also incorporate further HSA functionality into our parameterization tool, such as constraint curves for preprogrammed bending and variable size unit cells. Further geometric exploration will lead to exciting downstream applications, such as improved manipulators and concentric tube robots.

ACKNOWLEDGMENTS

This work was supported by the Texas Robotics Industrial Affiliate Program.

References

[1] X. Zheng, Y. Jiang, M. Mete, J. Li, I. Watanabe, T. Yamada, and J. Paik, "Metamaterial robotics," *Science Robotics*, vol. 10, no. 108, p. eadx1519, Nov. 2025.

[2] A. Rafsanjani, K. Bertoldi, and A. R. Studart, "Programming soft robots with flexible mechanical metamaterials," *Science Robotics*, vol. 4, no. 29, p. eaav7874, Apr. 2019.

[3] J. I. Lipton, R. MacCurdy, Z. Manchester, L. Chin, D. Cellucci, and D. Rus, "Handedness in shearing auxetics creates rigid and compliant structures," *Science*, vol. 360, no. 6389, pp. 632–635, 2018.

[4] A. G. Mark, S. Palagi, T. Qiu, and P. Fischer, "Auxetic metamaterial simplifies soft robot design," in *2016 IEEE International Conference on Robotics and Automation (ICRA)*, May 2016, pp. 4951–4956.

[5] A. Sedal, M. Kohler, G. Agbofode, T. Y. Moore, and S. Kota, "Emergent Sequential Motion Through Compliant Auxetic Shells," in *2023 IEEE/RSJ International Conference on Intelligent Robots and Systems (IROS)*, Oct. 2023, pp. 10 238–10 244.

[6] B. Zhang, Z. Meng, X. Yang, Y. Zhang, T. Chen, Y. Chen, and Y. Wang, "Multistable Soft Robots Assembled from Bistable Auxetic Building Blocks," *Advanced Intelligent Systems*, vol. 7, no. 4, p. 2400529, 2025.

[7] Q. Pan, S. Chen, F. Chen, and X. Zhu, "Programmable soft bending actuators with auxetic metamaterials," *Science China Technological Sciences*, vol. 63, no. 12, pp. 2518–2526, Dec. 2020.

[8] L. Chin, J. Lipton, R. MacCurdy, J. Romanishin, C. Sharma, and D. Rus, "Compliant electric actuators based on handed shearing auxetics," in *2018 IEEE International Conference on Soft Robotics (RoboSoft)*. Livorno: IEEE, Apr. 2018, pp. 100–107.

[9] T. Kim, E. A. Dunn, and R. L. Truby, "Clutchable Soft Actuators Produce Rapid, High-Power Movements in Robotic Artificial Musculoskeletal Systems," *IEEE Robotics and Automation Letters*, vol. 11, no. 3, pp. 3063–3070, Mar. 2026.

[10] P. Kaarthik, M. E. Bayer, T. Kim, and R. L. Truby, "Miniaturized and Motorized: Fast, Architected Soft Robotic Actuators via Molded Thermoplastic Elastomers," in *2025 IEEE 8th International Conference on Soft Robotics (RoboSoft)*, Apr. 2025, pp. 1–7.

[11] X. Zhang, M. Baggetta, C. Piazza, and G. Berselli, "A Single-Servo Gear-Coupled HSA Gripper: Finite Element Evaluation of Material Hardness and Thickness on Grip Performance," in *2025 IEEE/ASME International Conference on Advanced Intelligent Mechatronics (AIM)*, July 2025, pp. 1–6.

[12] L. Chin, M. C. Yuen, J. Lipton, L. H. Trueba, R. Kramer-Bottiglio, and D. Rus, "A Simple Electric Soft Robotic Gripper with High-Deformation Haptic Feedback," in *2019 International Conference on Robotics and Automation (ICRA)*. Montreal, QC, Canada: IEEE, May 2019, pp. 2765–2771.

[13] M. Stölzle, S. S. Baberwal, D. Rus, S. Coyle, and C. D. Santina, "Guiding Soft Robots with Motor-Imagery Brain Signals and Impedance Control," in *2024 IEEE 7th International Conference on Soft Robotics (RoboSoft)*, Apr. 2024, pp. 276–283.

[14] S. Thomas, A. Garg, and J. Lipton, "Torque-Transmitting Architected Metamaterials for Flexible and Extendable Tubular Robotics," *Advanced Intelligent Systems*, vol. 8, no. 2, p. 2500110, 2026.

[15] R. L. Truby, L. Chin, and D. Rus, "A Recipe for Electrically-Driven Soft Robots via 3D Printed Handed Shearing Auxetics," *IEEE Robotics and Automation Letters*, vol. 6, no. 2, pp. 795–802, Apr. 2021.

[16] I. Good, T. Brown-Moore, A. Patil, D. Revier, and J. I. Lipton, "Expanding the Design Space for Electrically-Driven Soft Robots Through Handed Shearing Auxetics," in *2022 International Conference on Robotics and Automation (ICRA)*, May 2022, pp. 10 951–10 957.

[17] Y. Hong, Y. Chi, S. Wu, Y. Li, Y. Zhu, and J. Yin, "Boundary curvature guided programmable shape-morphing kirigami sheets," *Nature Communications*, vol. 13, no. 1, p. 530, Jan. 2022.

[18] N. Lobontiu, *Compliant Mechanisms: Design of Flexure Hinges*. CRC Press, Dec. 2002.

[19] L. L. Howell, "Introduction to Compliant Mechanisms," in *Handbook of Compliant Mechanisms*. John Wiley & Sons, Ltd, 2013, ch. 1, pp. 1–13.

[20] Y. Tian, B. Shirinzadeh, D. Zhang, and Y. Zhong, "Three flexure hinges for compliant mechanism designs based on dimensionless graph analysis," *Precision Engineering*, vol. 34, no. 1, pp. 92–100, Jan. 2010.

[21] *TPU 85A Bambu Filament Technical Data Sheet V1.0*, Bambu Lab, Shenzhen, China, 2026.

[22] *PLA Bambu Filament Technical Data Sheet V3.0*, Bambu Lab, Shenzhen, China, 2026.

[23] Y.-X. Xu and J.-Y. Juang, "Measurement of nonlinear poisson's ratio of thermoplastic polyurethanes under cyclic softening using 2d digital image correlation," *Polymers*, vol. 13, no. 9, p. 1498, 2021.